Histol Histopathol (1997) 12: 701-718

Histology and Histopathology

Postnatal morphologic changes and glial fibrillary acidic protein immunoreactivity in the anteroventral cochlear nucleus of the acoustically-deprived gerbil

S.M. Yu and S.J. Du

Institute of Anatomy and Department of Anatomy, National Yang-Ming University, Taipei, Taiwan, Republic of China

Summary. This study investigated the morphological changes and glial fibrillary acidic protein immunoreactivity (GFAP-IR) in the anteroventral cochlear nucleus (AVCN) of acoustically-deprived gerbils during postnatal development. The mongolian gerbil, *Meriones unguiculatus*, had been acoustically deprived on the right side or left side by a surgical ligation of the external auditory canal at postnatal day 12-14. No discernible microcysts were located in the ipsilateral AVCN at one, three, six and nine months after monaural ligation. Also, no discernible microcysts were located in the contralateral AVCN at one and three months after monaural ligation. Numerous microcysts were located in the contralateral AVCN at six months after monaural ligation and were slightly reduced in number at nine months after monaural ligation. Some of the microcysts closely apposed to and connected with the blood vessels through a leakage route or channel. A foamy region was found in the superficial granule cell cap of the AVCN. The foamy region became evident in the ipsilateral AVCN at three months after monaural ligation. However, the foamy region became evident in the contralateral AVCN at three and nine months after monaural ligation. Vacuoles were mainly found in the neuronal cells at the junction of the superficial and deep layers in the AVCN. These vacuoles were found in the contralateral AVCN at one, three, six, and nine months after monaural ligation. However, vacuoles were found in the ipsilateral AVCN only at three months after monaural ligation. Morphological changes of the myelin sheath were found to be more severe in the contralateral AVCN than in the ipsilateral. GFAP-IR was located in the superficial layer of the contralateral AVCN at three and nine months after monaural ligation. However, GFAP-IR was found in the superficial and deep layers of the ipsilateral AVCN at three and nine months after monaural ligation. GFAP-IR was also found in the superficial layers of the ipsilateral AVCN at six months after monaural ligation. Microcysts are presumably derived from the detachment of the myelin sheath from the retracted axons, protrusion of the myelin sheath, and disruption of the myelin sheath. The major conclusions were that (1) microcysts were greatly reduced following acoustical ligation during postnatal development, and (2) blood vessels and GFAP-immunoreactive astrocytes may be involved in the depletion of microcysts for maintaining the homeostasis of the microenvironment in the cochlear nuclei.

Key words: Anteroventral cochlear nucleus, Electron microscopy, External auditory occlusion, Glial fibrillary acidic protein, Immunocytochemistry

Offprint requests to: Dr. Shang-Ming Yu, Institute of Anatomy, National Yang-Ming University, 155, Section 2, Lee-Nung Street, Shih-Pai, Taipei, Taiwan 11221, Republic of China

Introduction

It has been shown that microcystic lesions are most evident in the posteroventral and anteroventral cochlear nuclei (PVCN and AVCN) of the Mongolian gerbil. These microcystic lesions are reported as a neurodegenerative disorder in the cochlear nucleus of the gerbil (Morest et al., 1986; Ostapoff et al., 1987; Statler et al., 1990). They resemble spongioform degeneration (McGinn and Faddis, 1987; Ostapoff and Morest, 1989). Such lesions are large holes, cavities or vacuoles and are also known as microcysts. The microcysts develop in the neuropil (McGinn and Faddis, 1987) or appear in the neuronal perikarya, degenerated axons and dendrites (Ostapoff and Morest, 1989). The number and size of the microcysts are greatly reduced either by the elevation of auditory thresholds (McGinn et al., 1990), or by conductive hearing loss induced by ligation of the external auditory canal (McGinn and Faddis, 1987, 1988; Faddis and McGinn, 1993). Furthermore absence of microcysts is found in older deaf animals (Woolf et al., 1987; Kitzes and Moore, 1989; Czibulka and Schwartz, 1991). The microcysts do not cause major changes in neuronal populations in the posteroventral cochlear nucleus (PVCN) (Schwartz and Karnofsky, 1988). Czibulka and Schwartz (1991) observed no

correlation between increasing microcyst numbers and decrease in cell number. Results of quantitative measurements also indicate no change in the number or density of the astrocyte distribution as a function of age or of acute unilateral deafening (Czibulka and Schwartz, 1993). It has further been shown that microcysts are most evident in the PVCN and posterior anteroventral cochlear nucleus (McGinn and Faddis, 1987; Statler et al., 1990; Yu, 1992). Immunocytochemical staining methods have been widely used for localizing neurotransmitters and protein markers in the cochlear nucleus. Glial fibrillary acidic protein (GFAP) is an intermediate filament of cytoskeletal protein and is considered a specific marker for astrocytes (Eng et al., 1971; Bignami et al., 1972; Riggs et al., 1995; Butt and Kirvell, 1996). Although astrocytes may be involved in modulating the neuronal activity, the distributions and patterns of GFAP-immunoreactivity (IR) have not been systematically reported in acoustically-deprived gerbils. Previous investigation shows that microcysts are not immunolabeled with GFAP (Faddis and McGinn, 1993). Conversely, microcysts are immunolabeled internally with astrocytic markers S-100 or GFAP (Czibulka and Schwartz, 1993). Little information is known about microcysts in the anteroventral cochlear nucleus (AVCN). The functional role and the origin of microcysts are still unclear. Therefore, the nature, content and development of microcysts in the cochlear nucleus remain unsolved at present.

The purpose of this investigation was to systematically examine the morphological changes and GFAP-IR of microcysts in the acoustically-deprived gerbil AVCN during postnatal development at the light and electron microscopic levels. Parts of the preliminary results from this study have been reported previously (Du et al., 1994; Yu and Du, 1995).

Materials and methods

Light microscopy and electron microscopy

The mongolian gerbil, *Meriones unguiculatus*, were received at three months of age from the National Breeding and Research Center of Laboratory Animals in the National Taiwan University and housed in standard vivarium facilities with room temperature (24-26 ºC) and lighting schedule (light on 0500-1900 h daily). Animals were mated and gerbil litters were acoustically deprived on the right side or left side by a ligation of the external auditory canal at postnatal day 12-14 (McGinn and Faddis, 1987). At 1 (n1=4, n2=3), 3 (n1=5, n2=3), 6 (n1=3, n2=3) and 9 (n1=8, n2=11) months after ligation, animals were anesthetized with sodium pentobarbital (30 mg/kg, i.p.) and sacrificed by cardiac perfusion with saline nitrite solution (0.9% NaCl, 0.1% $NaNO_2$). The number within brackets indicates the number of animals in that age group used for right monaural ligation (n1) or left monoaural ligation (n2) of the external auditory canal.

Animals were fixed in a modification of McLean and Nakane's fixative (1974) of 6% paraformaldehyde-lysine-periodate in 0.1M phosphate buffer (Yu, 1993a,b). The brains were removed from the skull, immersed in the same fixative overnight, embedded in agar and sliced with a DTK-1000 Microslicer at 250 μm. The brain slices were thoroughly rinsed in the same phosphate buffer for one hour and were then immersed in 1% osmium tetroxide, dehydrated in a graded series of ethanol, immersed in propylene oxide, infiltrated with Epon-Araldite/propylene oxide (1:1), and cured in freshly-prepared Epon-Araldite resin through an improved flat embedding technique (Yu and Schwartz, 1989). After polymerization, the sliced tissues were sectioned at 1-2 μm with glass knives on an ultramicrotome for light microscopy. The sections were mounted on slides within a circle marked by a diamond pen. The slides were stained with toluidine blue for light microscopy. For electron microscopy ultrathin sections (60-90 nm thickness) were cut on an ultramicrotome, placed on copper or nickle grids, and examined with a JEOL electron microscope (JEM-2000EXII).

Immunocytochemistry

The plastic-embedded tissues were sectioned at 1-2 μm with glass knives on an ultramicrotome for light immmunocytochemical staining. The sections were mounted on slides within a circle marked by a diamond pen. The sections were deplasticized in saturated sodium hydroxide in absolute alcohol (1:3) for 7 minutes, immersed in 3% hydrogen peroxide, and incubated in 10% normal goat serum (NGS) in phosphate-buffered saline (PBS) for 10 minutes. Immunocytochemical staining was performed as follows: (1) incubation in rabbit anti-glial fibrillary acidic protein (A/GFAP, diluted 1:50-1:100, Zymed Laboratories Inc., CA) for 14-16 hours, in 0.01M PBS; (2) incubation in biotinylated goat anti-rabbit IgG (Vectastain kit, Vector Labs) for 2 hours; (3) incubation in ABC reagent (avidin-biotin-peroxidase complex, Vectastain kit, Vector Labs) for 2 hours; (4) treatment with 3,3'-diaminobenzidine tetrahydrochloride (Sigma, 0.3 mg/ml) in 0.05M Tris buffer containing 0.002% hydrogen peroxide, pH 7.6 until immunoreactive sites were visible. All incubations were carried out at room temperature. Finally, the sections were dehydrated in ethanol, cleared in xylene, and coverslipped.

In control samples, the first antibody, A/GFAP was replaced by (1) normal rabbit serum or (2) PBS.

Results

Light microscopy

The AVCN consisted of a superficial layer and a deep layer. The superficial layer covered the lateral surface of the AVCN. A lateral angle at the superficial layer divided the lateral surface into a dorsal small cell

cap (a third of the lateral surface) and a ventral portion (two thirds). This lateral angle also marked the ventral limit of the lateral recess of the fourth ventricle. After monaural ligation, microcysts remained in the contralateral AVCN but were greatly reduced in the ipsilateral AVCN. At one month after monaural ligation, no discernible microcysts were found in the superficial and deep layers of the contralateral (Fig. 1A,B) and ipsilateral (Fig. 1C,D) AVCN of the monaurally deprived gerbils. A foamy region was located in the superficial granule cell cap (Fig. 1B,D). Neuronal vacuoles were located in the peripheral cytoplasm of the neuronal cells at the junction of the superficial granule cell cap and the deep layer in the contralateral AVCN (Fig. 1B). At three months after monaural ligation, no discernible microcyst was found in the contralateral (Fig. 2A,B) and ipsilateral (Fig. 2C,D) AVCN. A foamy region became evident in the superficial granule cell cap of the contralateral (Fig. 2B) and ipsilateral (Fig. 2D) AVCN. A few vacuoles were found in the neuronal cells adjacent to the granule

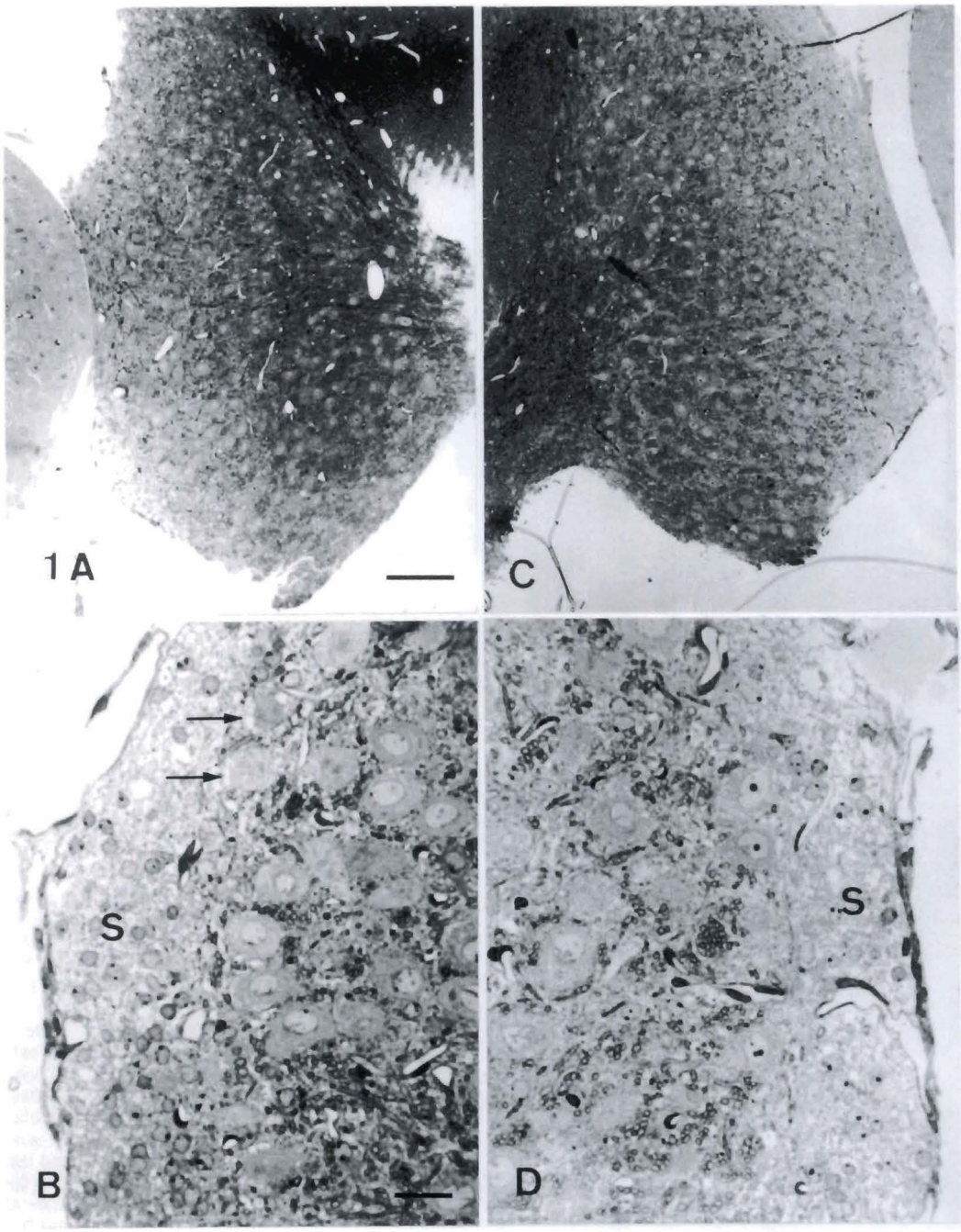

Fig. 1. Light micrographs of the left AVCN **(A,B)** and right AVCN **(C,D)** at one month after right ligation. No discernible microcysts are found in the AVCN **(A,C)**. A foamy region is located in the superficial granule cell cap (S) of the left **(B)** and right AVCN **(D)**. The neuronal cells of the superficial granule cell cap and the deep layer contains vacuoles (arrows) in the cytoplasm near the peripehral plasmalemma in the left AVCN **(B)**. Scale bar: 100 μm for A and C, and 25 μm for B and D.

cell cap in the contralateral (Fig. 2B) and ipsilateral (Fig. 2D) AVCN. At six months after monaural ligation, numerous microcysts were found in the deep ventral layer of the contralateral AVCN (Fig. 3A). Some of the microcysts closely apposed to the blood vessel (Fig. 3A). No discernible microcysts were found in the ipsilateral AVCN (Figs. 3C). A foamy region was slightly reduced in the contralateral (Fig. 3B) and ipsilateral (Fig. 3D) AVCN. Vacuoles became more evident in the neuronal cells adjacent to the superficial granule cell cap in the contralateral AVCN (Fig. 3B) than those at three months. No vacuoles were found in the ipsilateral AVCN (Fig. 3D). At nine months after monaural ligation, microcysts were reduced in number in the contralateral (Fig. 3A). No discernible microcysts were found in the ipsilateral AVCN (Fig. 4C). A foamy region became more evident in the superficial granule cell cap of the contralateral AVCN (Fig. 4B) than that of the ipsilateral (Fig. 4D). Numerous vacuoles remained in the neuronal cell adjacent to the superficial granule cell cap in the

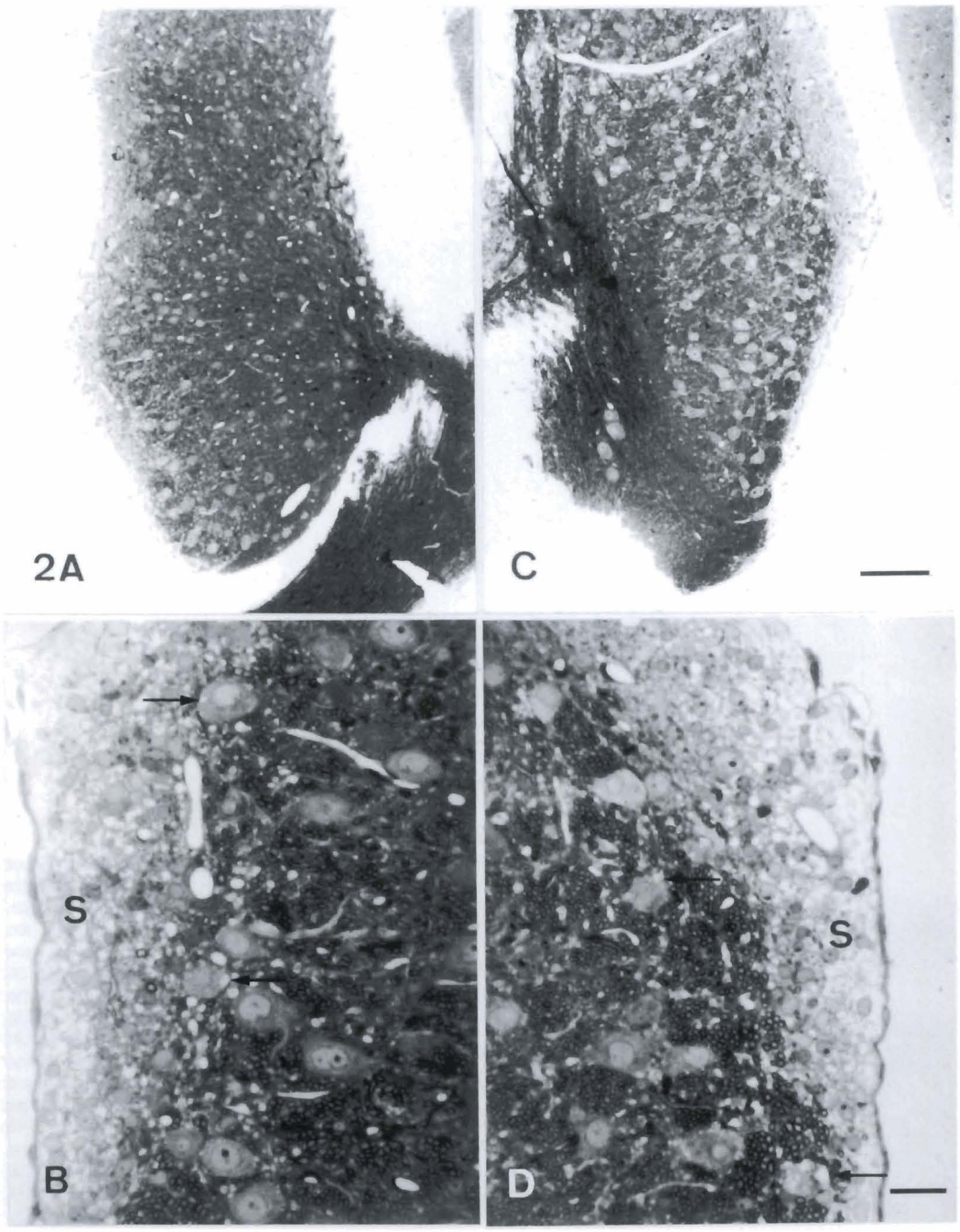

Fig. 2. Light micrographs of the left AVCN **(A,B)** and right AVCN **(C,D)** at three months after right ligation. No discernible microcysts are found in the AVCN **(A,C)**. A foamy region becomes evident in the superficial granule cell cap (S) of the left **(B)** and right **(D)** AVCN. A few vacuoles are found in the neuronal cells (arrows) adjacent to the superficial granule cell cap (S) in the left **(B)** and right **(D)** AVCN. Scale bar: 100 μm for A and C, and 25 μm for B and D.

contralateral AVCN (Fig. 4B). No vacuoles were found in the ipsilateral (Fig. 4D) AVCN.

Electron microscopy

At one month after monaural ligation, vacuoles were found in the cytoplasm near the periphral plasmalemma in the neuronal cell of the contralateral AVCN (Fig. 5A). A foamy region corresponded to edematous dendrites (Fig. 5B). Protrusion and disruption of the myelin sheath were found in the contralateral AVCN. Occasionally a microcyst was found among myelinated nerve fibers and it also contained membranous structures (Fig. 5C). A fraction of the myelin sheath showed slight protrusion into the microcyst from the neighboring myelinated nerve fiber. Vacuoles were also found in the neuronal cell of the ipsilateral AVCN (Fig. 5D). Disruption of the myelin sheath was also found in the ipsilateral AVCN (Fig. 5E). A foamy region was edematous dendrites and showed the protrusion of the myelin sheath into the dendrites from the neighboring myelinated nerve fiber (Fig. 5F).

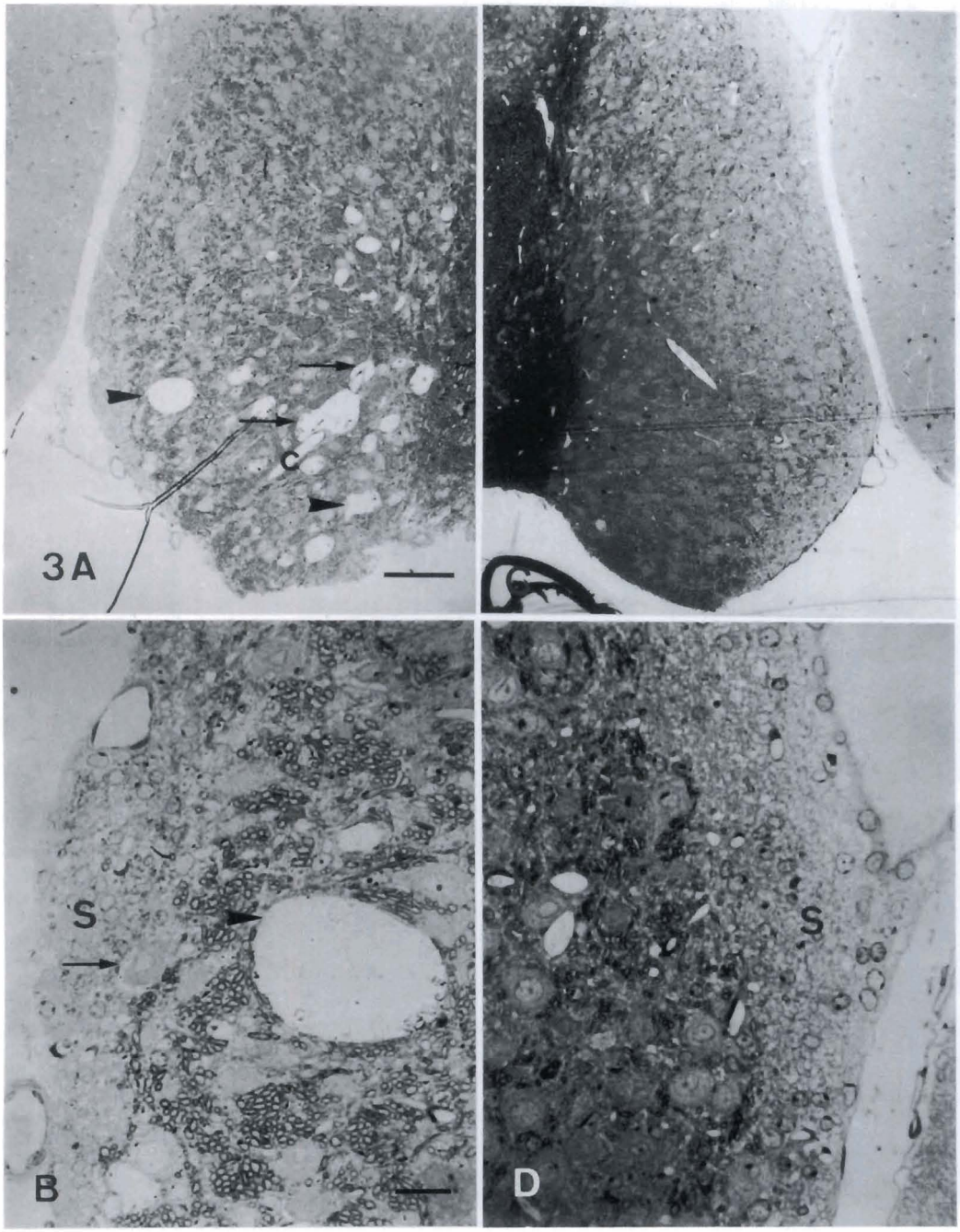

Fig. 3. Light micrographs of the left AVCN **(A,B)** and right AVCN **(C,D)** at six months after right ligation. Numerous microcysts (arrowheads) are found in the deep ventral layer of the left AVCN **(A)**. Note that the microcysts (arrows) closely contacted blood vessels (C). No microcysts are found in the right AVCN **(C)**. A foamy region is slightly reduced in the left **(B)** and right **(D)** AVCN. Numerous vacuoles (arrow) are found in the neuronal cells adjacent to the superficial granule cell cap (S) of the left AVCN **(B)**. No vacuoles are found in the right AVCN **(D)**. Scale bar: 100 μm for A and C, and 25 μm for B and D.

At three months after monaural ligation, a few microcysts were found in close contact with the neuronal cell in the contralateral AVCN (Fig. 6A). These microcysts were probably derived from edematous dendrites. A blood vessel contained a membranous structure in its lumen and a vacuole in the cytoplasm of the endothelial cell. The adjacent pericyte contained several multivesicular bodies (Fig. 6B). This blood vessel may be involved in a phagocytic process and in the maintenance of the microenvironment of the microcysts. Detachment of the myelin sheath from the retracted axons was found in the contralateral AVCN. Disruption of the myelin sheath was found in the contralateral AVCN (Fig. 6C) and was also found in the ipsilateral AVCN (Fig. 6D). Vacuoles were found in the cytoplasm of the neuronal cell near the periphral plasmalemma in the ipsilatral AVCN (Fig. 6E). The myelin sheath protruded into the myelinated nerve fiber in the ipsilateral AVCN (Fig. 6F). The foamy region corresponded to edematous dendrites or vacuoles. The

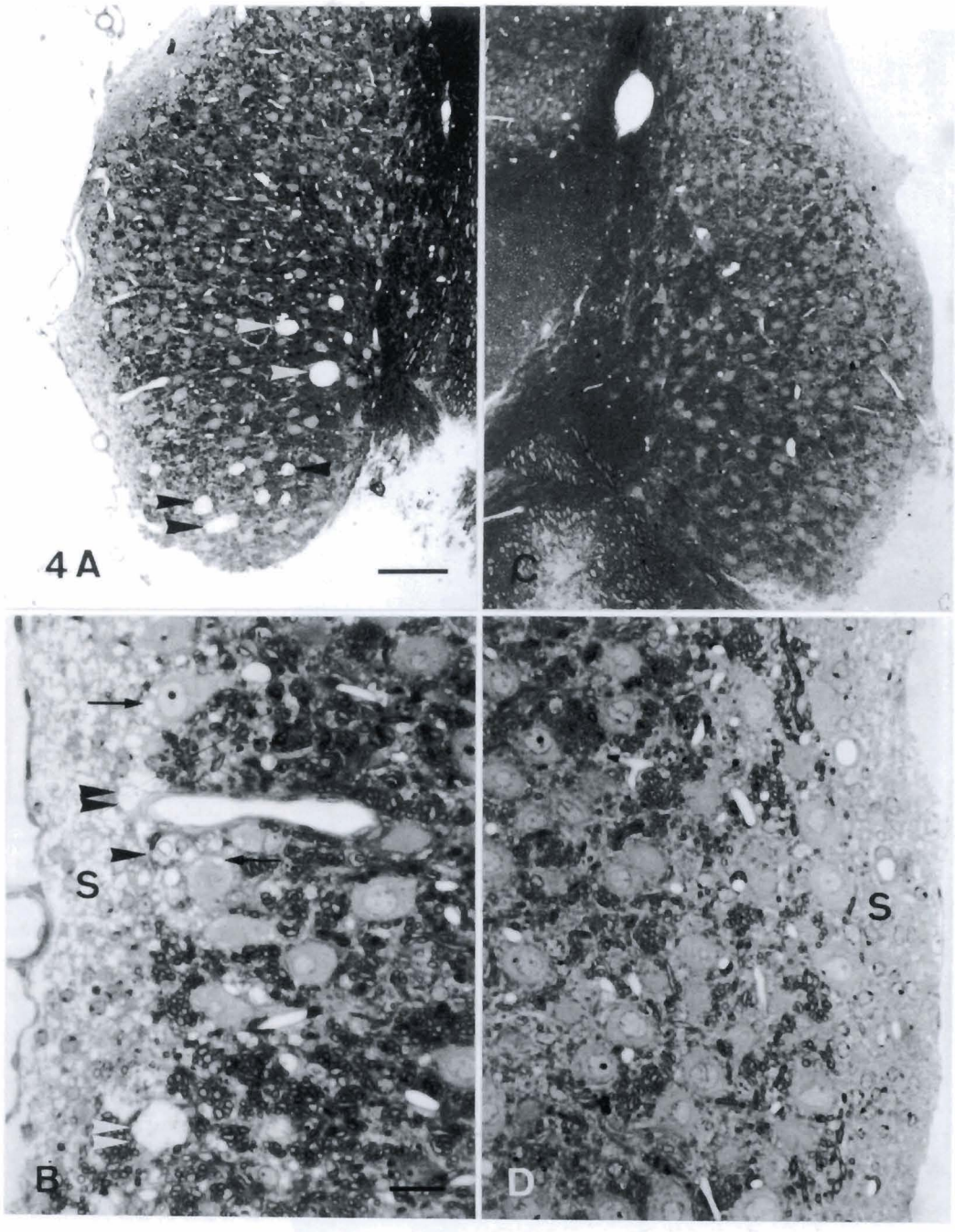

Fig. 4. Light micrographs of the left AVCN **(A,B)** and right AVCN **(C,D)** at nine months after right ligation. Numerous microcysts (arrows) remained in the left AVCN **(A)**. Some of the microcysts (double arrowheads) are found at the junction of the superficial granule cell cap and the deep layer, and the vacuoles (arrows) in the neuronal cells of the left AVCN **(B)**. Note that the vacuole (single arrowhead) contains vesicles. A foamy region is more evident in the superficial granule cell cap (S) of the left AVCN **(B)** than in that of the right AVCN **(D)**. No vacuoles are found in the right AVCN **(D)**. Scale bar: 100 μm for A and C, and 25 μm for B and D.

vacuoles closely contacted the nuclei of the superficial granule cell (Fig. 6G) or were found in the cytoplasm of the granule cell near the peripheral plasmalemma (Fig. 6H) in the superficial layer of the ipsilateral AVCN. Edematous dendrites were found between myelinated nerve fibers in the superficial cell layer (Fig. 6I). These edematous dendrites frequently contained a large vacuole associated with the disruption of the myelin sheath.

At six months after monaural ligation, numerous microcysts were found in the contralateral AVCN (Fig. 7). Edematous dendrites closely contacted the neuronal cell in the contralateral AVCN (Fig. 7A). Such dendrites contained large and distorted mitochondria. Some of the dendrites contained a membranous structure (Fig. 7B). A blood vessel contained a thin cytoplasmic rim and a membranous structure in its lumen. A vacuole also closely contacted an adjacent blood vessel (Fig. 7C). A microcyst was also closely associated with the blood vessel. One kind of large microcyst with a distinct boundary was found in the contralateral AVCN (Fig. 7D). This microcyst contained a lot of dilated vesicles and mitochondria. Most of the mitochondria were located between the vesicles and some of them were found within the vesicles. These large vesicles seemed to be coalesced with the small vesicles. This microcyst was also associated with a nucleus of a glial cell. It was not possible to trace the cytoplasmic processes of this glial cell. This glial cell was presumably an oligodendrocyte and the vesicles were probably derived from the disruption of the myelin sheath. Another large microcyst without a distinct boundary was found in the ipsilateral AVCN (Fig. 7E). The microcyst contained a lot of the membranous structure, cytoplasmic debris including ribosomes, and a red blood cell. The adjacent retracted axon showed detachment of the myelin sheath. Adjacent to a longitudinally-sectioned myelinated nerve fiber, two glial cells closely contacted each other and no distint cell boundary was found between them (Fig. 7F). Protrusion of the myelin sheath was found in the cytoplasm of the glial cells.

At nine months after monaural ligation, edematous dendrites corresponded to the foamy region and were evident in the superficial granule cell cap of the contralateral AVCN (Fig. 8A). A myelin sheath protruded into a edematous dendrite. Detachment of the myelin sheath from the retracted axon was severe (Fig. 8B). A lot of small vesicles were found in the retracted axon. Severe detachment and disruption of the myelin sheath were found in the contralateral AVCN (Fig. 8C). The axoplasm of the retracted axon became irregular and smaller. Some of axoplasm was occupied by a lot of vesicles and became a thin mesh-like rim. Vacuoles (Fig. 8D) and edematous dendrites (Fig. 8E) were found in the superficial layer of the ipsilateral AVCN. Some of the vacuoles coalesced to form a dumbbell-shaped vacuole (Fig. 8D). A microcyst with a distinct boundary contained distorted mitochondria and the protruded myelin sheath adjacent to an intensely-stained glial cell (Fig. 8F). Another irregular microcyst without a circumscribed boundary was found between the glial cell and a blood vessel.

In the contralateral AVCN, a blood vessel contained a smooth and regular profile at one month after monaural ligation (Fig. 9A). A few microcysts were closely associated with this blood vessel. At three months after monaural ligation, a blood vessel contained a membranous structure in its lumen and a pericyte contained multivesicular bodies (Fig. 6B). At six months after monaural ligation, a thin cytoplasm of the endothelial cell protruded into the lumen of a blood vessel. This thin cytoplasmic rim seemed to separate the lumen into two smaller compartments (Fig. 9B). An intact pericyte resided at the periphery of the blood vessel. Some of the blood vessels contained several membranous structures (Fig. 7C). At nine months after monaural ligation, a blood vessel contained a membranous structure in the lumen and an endothelial cell was reduced in thickness (Fig. 9C). A pericyte became irregular and contained a vacuole. A microcyst closely contacted the blood vessel.

In summary, we have shown that microcysts were greatly reduced following acoustical ligation during postnatal development. No discernible microcysts were located in the ipsilateral AVCN at one, three, six and nine months after monaural ligation. Also, no discernible microcysts were found in the contralateral AVCN at one and three months after monaural ligation. Numerous microcysts were located in the contralateral AVCN at six months after monaural ligation and were slightly reduced in number at nine months after monaural ligation. Some of the microcysts closely apposed to and connected with blood vessels. A foamy region was found in the superficial granule cell cap of the AVCN. The foamy region became evident in the ipsilateral AVCN at three months after monaural ligation. However, the foamy region became evident in the contralateral AVCN at three and nine months after monaural ligation. Vacuoles were mainly found in neuronal cells at the junction of the superficial and deep layer in the AVCN. These vacuoles were found in the contralateral AVCN at one, three, six, and nine months after monaural ligation. However, vacuoles were found in the ipsilateral AVCN only at three months after monaural ligation. Morphological changes of the myelin sheath were found to be more severe in the contralateral AVCN than in the ipsilateral.

GFAP-immunoreactivity

(A) The superficial layer of the AVCN

No discernible GFAP-immunoreactivity (IR) was immunolabeled in the contralateral (Fig. 10A) or ipsilateral (Fig. 10B) AVCN at one month after monaural ligation. GFAP-IR was immunolabeled in the contralateral (Fig. 10C) and ipsilateral (Fig. 10D) AVCN at three months after monaural ligation. GFAP-IR was

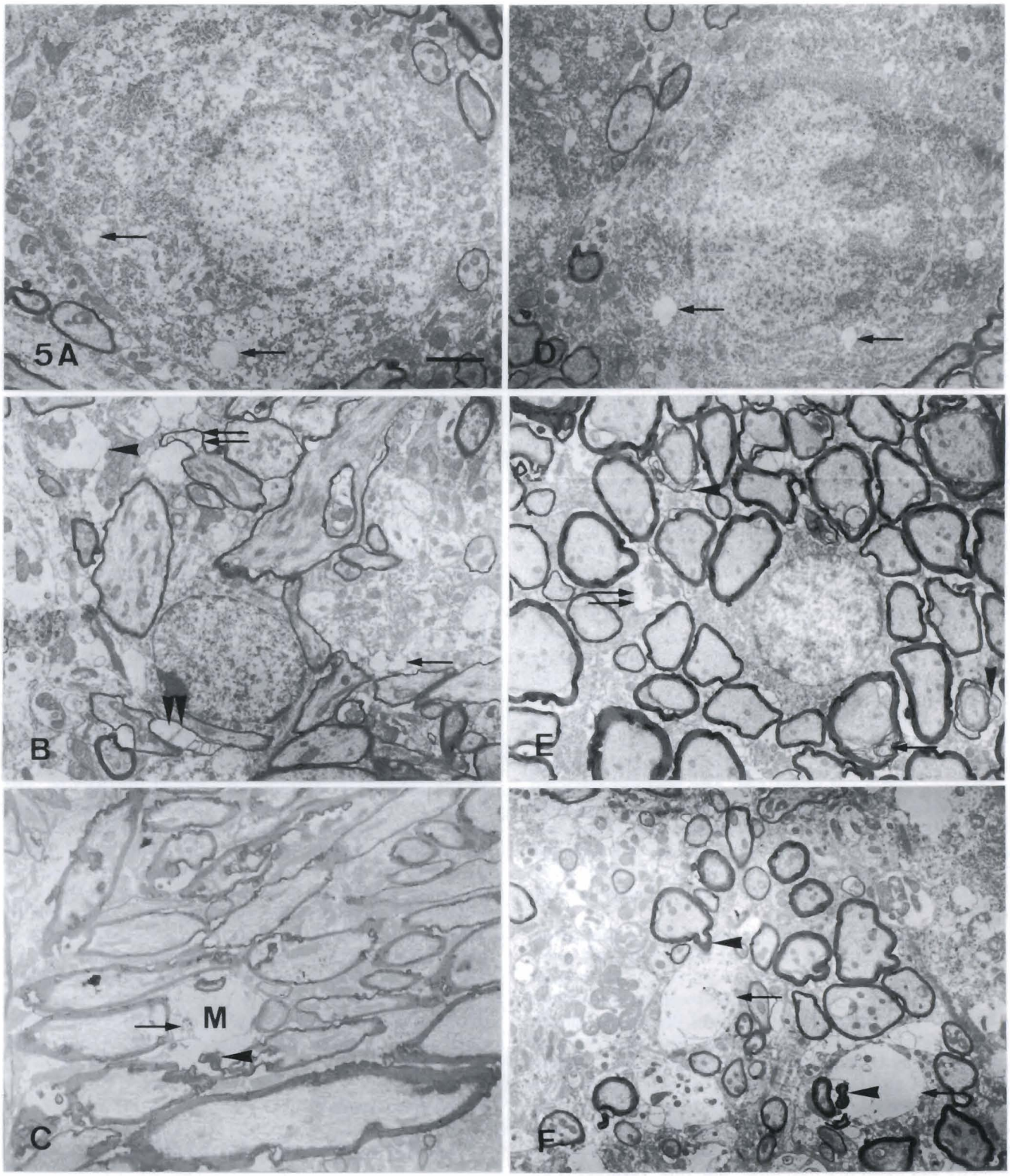

Fig. 5. Electron micrographs of the left AVCN **(A,B,C)** and right AVCN **(D,E,F)** at one month after right ligation. Vacuoles (arrows) are found in the neuronal cell of the left AVCN **(A)**. The foamy region corresponds to edematous dendrites (arrowhead) **(B)**. Note the protrusion (double arrows) and the disruption (double arrowheads) of the myelin sheath and the vacuoles (arrow). A microcyst (M) is found in the neuropil and surrounded by myelinated nerve fibers **(C)**. Note the membranous structure (arrow) and the protrusion of myelin sheath (arrowheads). Vacuoles are also found in the neuronal cell of the right AVCN **(D)**. Disruption (single arrow) and partial protrusion (arrowheads) of the myelin sheath are found in the right AVCN **(E)**. Note the edematous dendrite (double arrows). The foamy region is edematous dendrites (arrows) and shows protrusion of the myelin sheath (arrowheads) into the dendrites from the neighboring myelinated nerve fiber **(F)**. Scale bar: 2 μm.

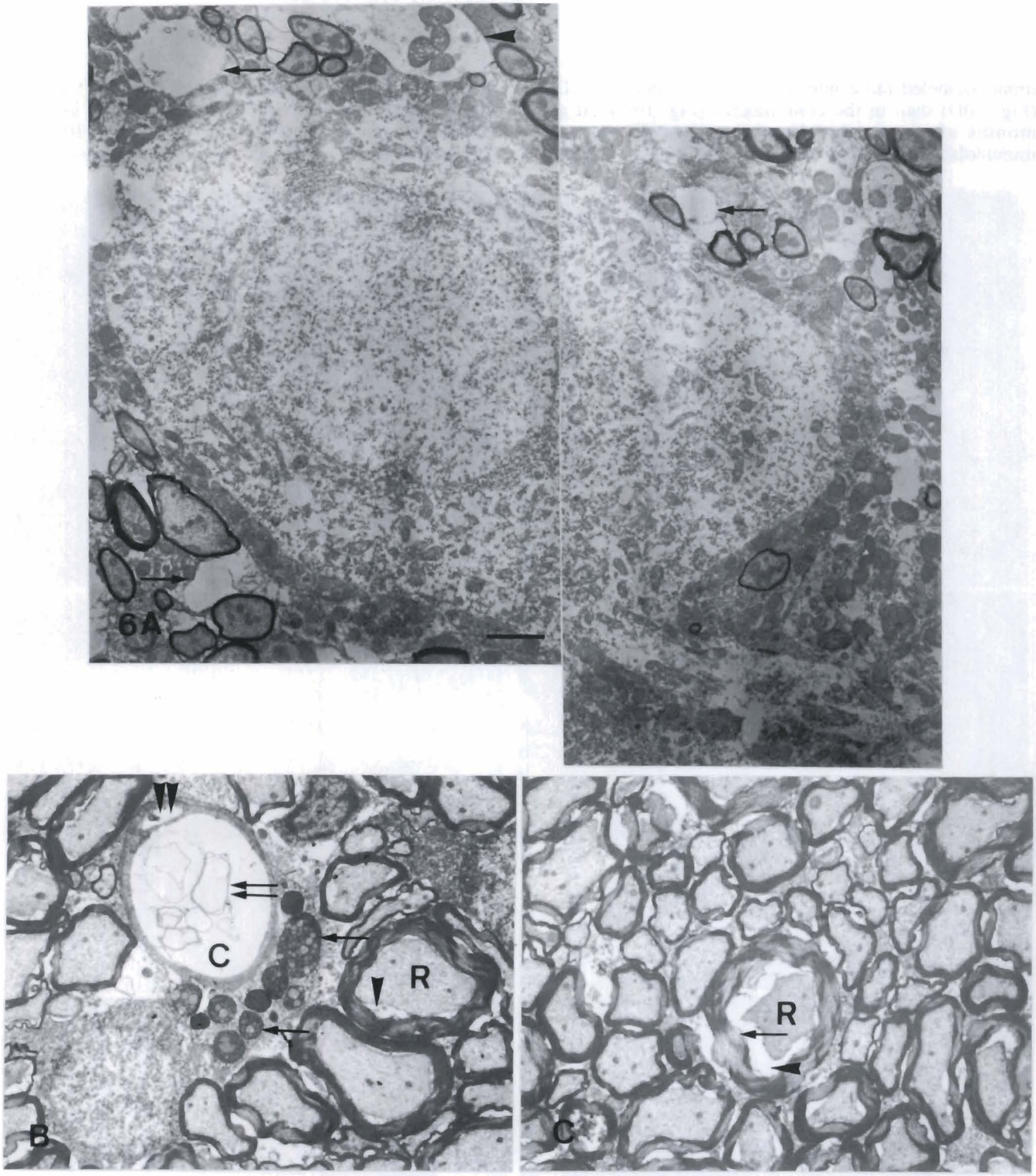

Fig. 6. Electron micrographs of the left AVCN **(A-C)** and right AVCN **(D-I)** at three months after right ligation. A few microcysts (arrows), probably derived from edematous dendrites, closely contact or are adjacent to a neuronal cell **(A)**. A blood vessel (C) contains a membranous structure (double arrows) in its lumen and a vacuole (double arrowheads) in the endothelial cell **(B)**. An adjacent pericyte contains several multivesicular bodies (single arrows). Note the detachment (single arrowhead) of the myelin sheath from the retracted axon (R). Disruption (arrow) and detachment (arrowhead) of the myelin sheath are found in the right AVCN **(C)**. Disruption of the myelin sheath (arrow) is found in the right AVCN **(D)**. Vacuoles (arrows) are found in the cytoplasm near the periphral plasmalemma in the ipsilateral AVCN **(E)**. The myelin sheath (arrows) protrudes into the myelinated nerve fiber in the ipsilateral AVCN **(F)**. Vacuoles (arrows) are closely contacting the nuclei (N) **(G)** or are found in the cytoplasm near the peripheral plasmmalemma **(H)** of the superficial granule cell in the right AVCN. Note the detachment (arrowhead) of the myelin sheath **(G)**. Edematous dendrites (arrows) corresponding to the foamy region are found in the neighboring cells **(I)**. Large vacuoles are frequently found in edematous dendrites (arrows) or are closely associated with the disruption of the myelin sheath (double arrowheads). Scale bar: 2 μm.

immunolabeled more intensely in the ipsilateral AVCN (Fig. 10D) than in the contralateral (Fig. 10C). At six months after monaural ligation, GFAP-IR was not immunolabeled in the contralateral AVCN (Fig. 10E) but was slightly reduced in the ipsilateral (Fig. 10F). At nine months after monaural ligation, GFAP-IR was immunolabeled in both the contralateral AVCN (Fig. 10G) and the ipsilateral (Fig. 10H). GFAP-IR was immunolabeled

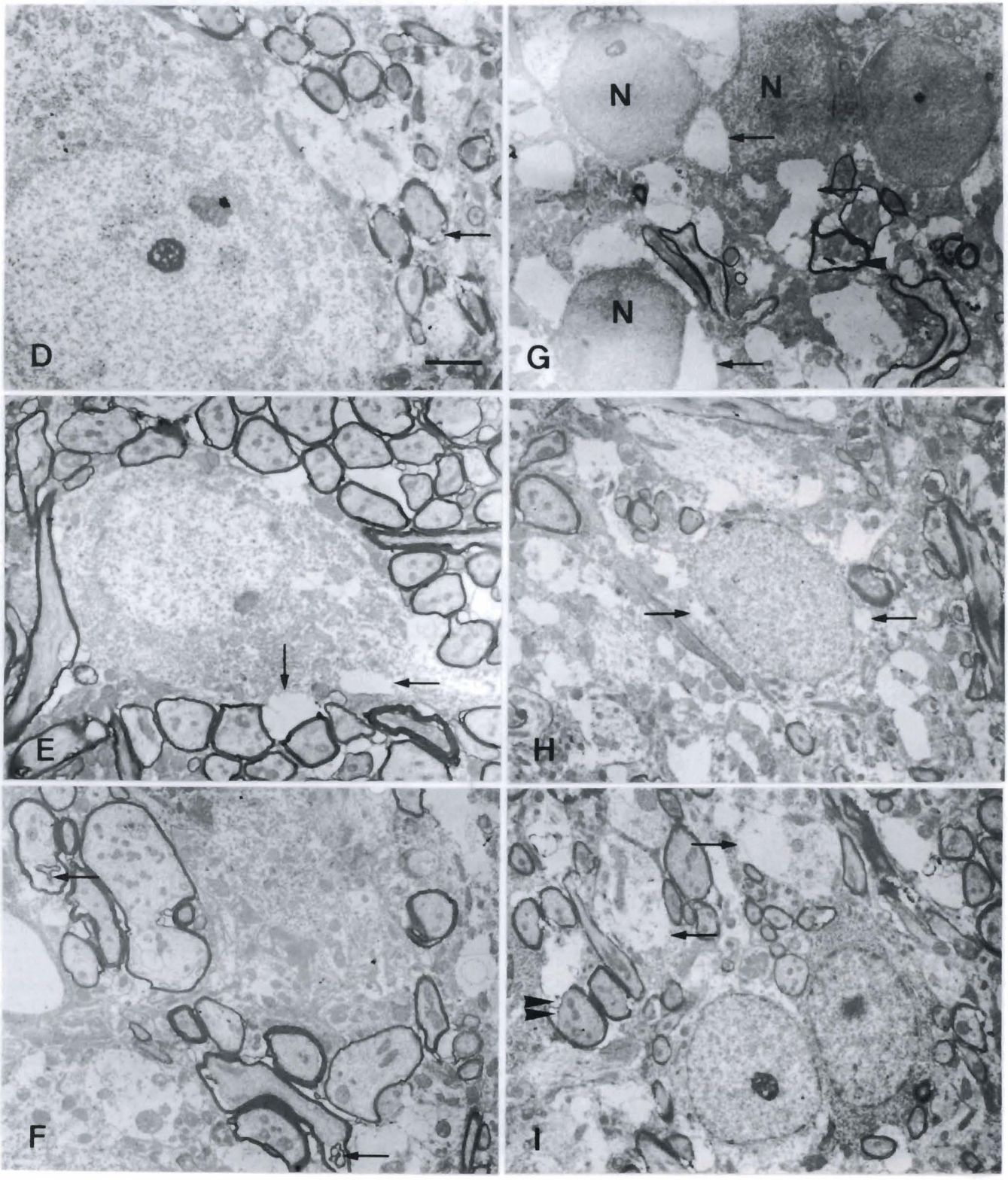

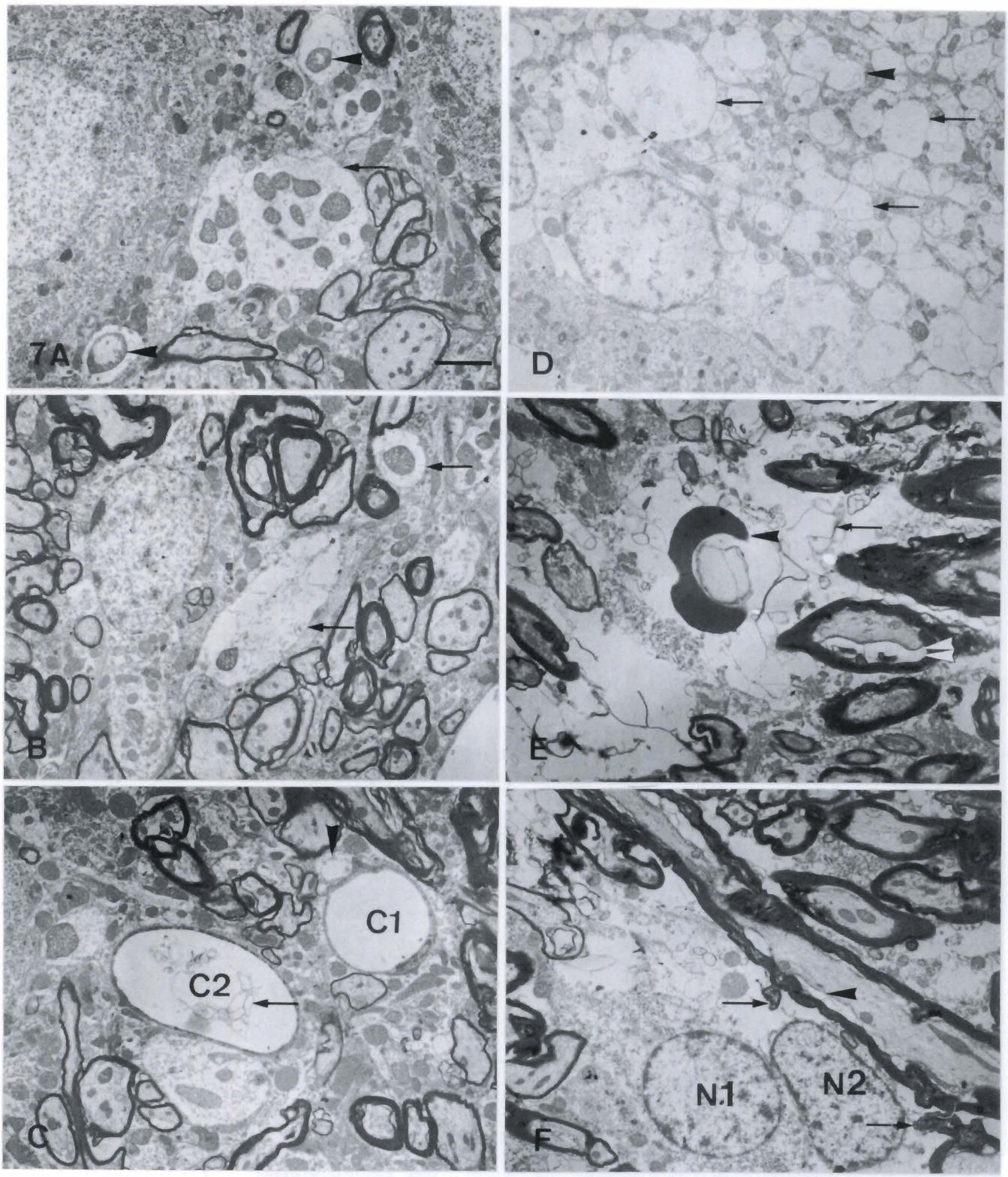

Fig. 7. Electron micrographs of the left AVCN **(A-D)** and right AVCN **(E,F)** at six months after right ligation. Edematous dendrites closely contact a neuronal cell in the left AVCN **(A)**. Note the large distorted mitochondria (arrowheads). The edematous dendrites (arrow) contains a membranous structure and mitochondria **(B)**. A vacuole closely contacts a blood vessel (C1). An adjacent blood vessel (C2) contains a thin cytoplasmic rim and a membranous structure (arrow) **(C)**. One kind of large microcyst with a distinct boundary contains a lot of dilated vesicles (arrows) and mitochondria **(D)**. The large vesicles (arrowhead) seem to be coalesced with the small vesicles. Another large microcyst without a distinct boundary is found in the right AVCN **(E)**. This microcyst contains a lot of the membranous structure (arrow), cytoplasmic debris including ribosomes, and a red blood cell (single arrowhead). Note the detachment of the myelin sheath (double arrowheads) from the retracted axon. The nuclei (N1 and N2) of two glial cells closely contact each other and no distinct cell boundary is found between them **(F)**. Note the detachment of the myelin sheath (arrowhead) and the protrusion of the myelin sheath (arrows) into the cytoplasm of the glial cells. Scale bar: 2 μm

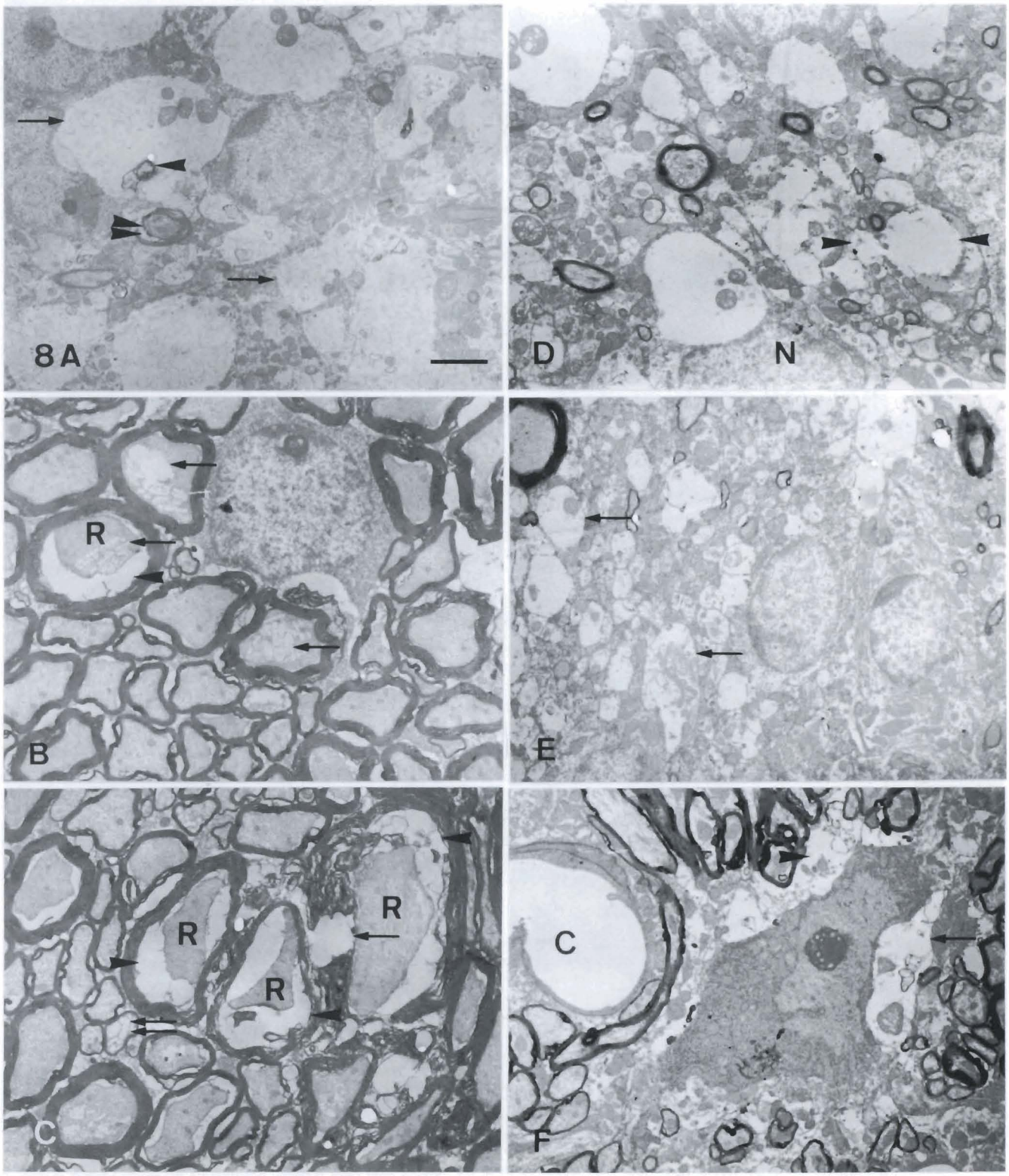

Fig. 8. Electron micrographs of the left AVCN **(A-C)** and right AVCN **(D-F)** at nine months after right ligation. Edematous dendrites corresponding to the foamy region are evident in the superficial granule cell cap of the left AVCN (**A**). Note the protrusion of the myelin sheath. Detachment of the myelin sheath (arrowhead) from a retracted axon is severe **(B)**. A lot of small vesicles (arrows) are found in the retracted axon (R). Severe detachment (arrowheads) and disruption (arrow) of the myelin sheath are found in the left AVCN **(C)**. The axoplasm of the retracted axon becomes irregular and smaller. Some of axoplasm is occupied by a lot of vesicles and becomes a thin mesh-like rim (double arrows). Vacuoles (arrowheads) and edematous dendrites (arrows) are found in the superficial granule cell cap of the right AVCN **(D,E)**. Some of the vacuoles coalesce to form a dumbbell-shaped vacuole **(D)**. A microcyst (arrow) with a distinct boundary contains distorted mitochondria and a protruded myelin sheath adjacent to a glial cell **(F)**. Another irregular microcyst (arrowhead) without a circumscribed boundary is found between the glial cell and a blood vessel (C). Scale bar: 2 μm.

more intensely in the ipsilateral AVCN (Fig. 10H) than in the contralateral (Fig. 10G).

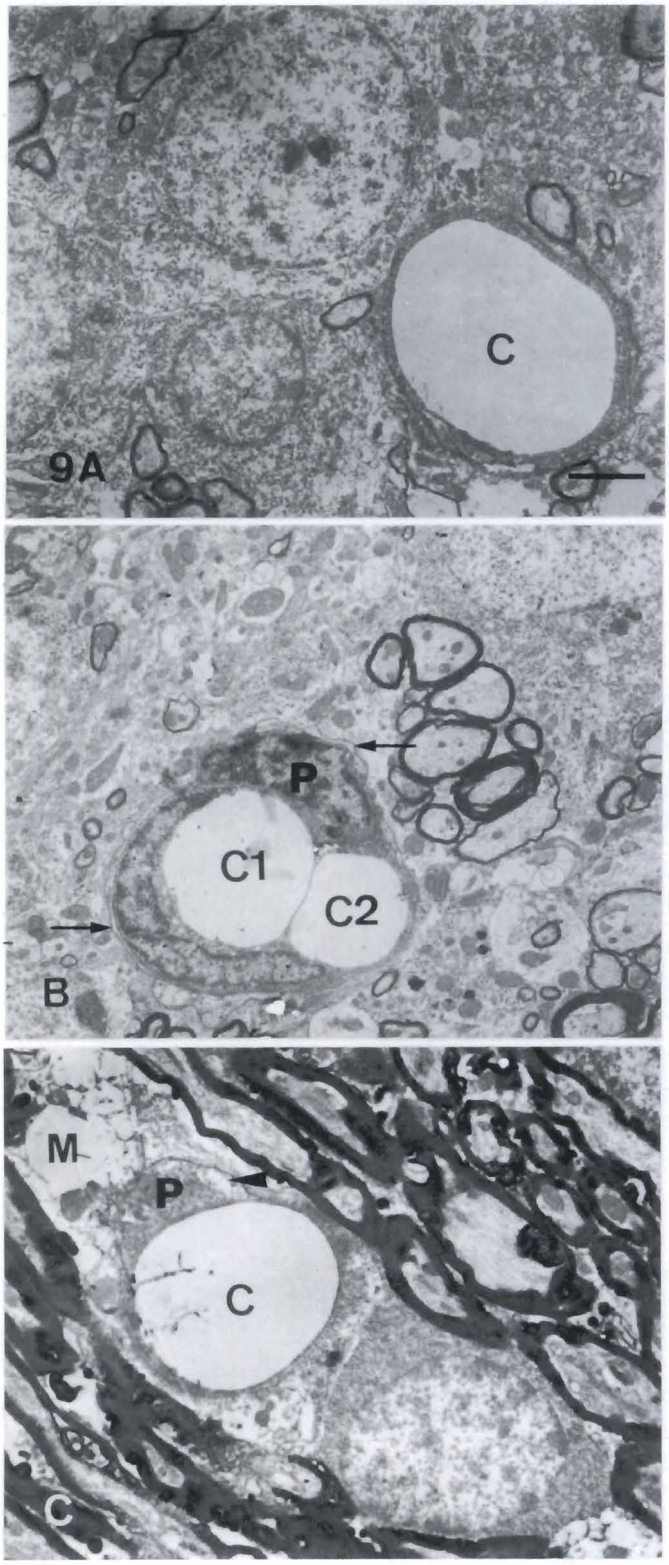

(B) The deep layer of the AVCN

No discernible GFAP-IR was immunolabeled in the contralateral (Fig. 11A) and ipsilateral (Fig. 11B) AVCN at one month after monaural ligation. At three months after ligation, GFAP-IR was not immunolabeled in the contralateral AVCN (Fig. 11C) but was immunolabeled in the ipsilateral (Fig. 11D). At six months after ligation, no discernible GFAP-IR was immunolabeled in the contralateral (Fig. 11E) and ipsilateral (Fig. 11F) AVCN. At nine months after ligation, GFAP-IR was not immunolabeled in the contralateral AVCN (Fig. 11G) but was immunolabeled in the ipsilateral (Fig. 11H).

In summary, GFAP-IR was located in the superficial layer of the contralateral AVCN at three and nine months after monaural ligation. However, GFAP-IR was located in the superficial and deep layer of the ipsilateral AVCN at three and nine months after monaural ligation. GFAP-IR was also located in the superficial layer of the ipsilateral AVCN at six months after monaural ligation.

Numerous microcysts were found in the contralateral AVCN at six months after monaural ligation. Some of the microcysts were closely associated with blood vessels in the deep layer of the AVCN. Microcysts connected with a blood vessel through a leakage route or channel (Fig. 12A,B). At this age, GFAP-IR was also located in the ependymal layer of the contralateral (Fig. 12C) and ipsilateral (Fig. 12D) AVCN.

Discussion

The modified fixative (Yu, 1993a,b), para-formaldehyde-lysine-periodate (PLP) (McLean and Nakane, 1974) and osmium, optimally preserves the prolactin immunoreactivity and cellular ultrastructure in rat pituitary glands. In this study, we perfused the gerbil brains with different concentrations (2%, 4% or 6%) of PLP and observed that 6% PLP was the best one to preserve the brain tissue by cardiac perfusion.

Microcysts (Ostapoff and Morest, 1989; Czibulka and Schwartz, 1991) are holes, cavities (Kitzes and Moore, 1989) or vacuoles (Yu, 1992) and are thought to be a spongioform lesion (McGinn and Faddis, 1987) or a dynamic process related to thedegree of auditory stimulation (Czibulka and Schwartz, 1991). A previous study (Yu and Ke, 1992) shows that microcysts are found

Fig. 9. Electron micrographs of the left AVCN **(A-C)** at one, six, and nine months after right ligation. A blood vessel (C) contains a smooth and regular profile at one month after right ligation **(A)**. A thin cytoplasm (arrowhead) of the endothelial cell protrudes into the lumen of a blood vessel at six months after right ligation **(B)**. This thin cytoplasmic rim seemed to separate the lumen into two smaller compartments (C1 and C2). Note the basement membrane (arrow) and the intact pericyte (P) residing at the periphery of the blood vessel. A blood vessel (C) contains a membranous structure in the lumen and the endothelial cell is reduced in thickness at nine months after right ligation **(C)**. Note the pericyte (P) becomes irregular and contains a vacuole (arrowhead). The microcyst (M) closely contacted the blood vessel. Scale bar: 2 μm.

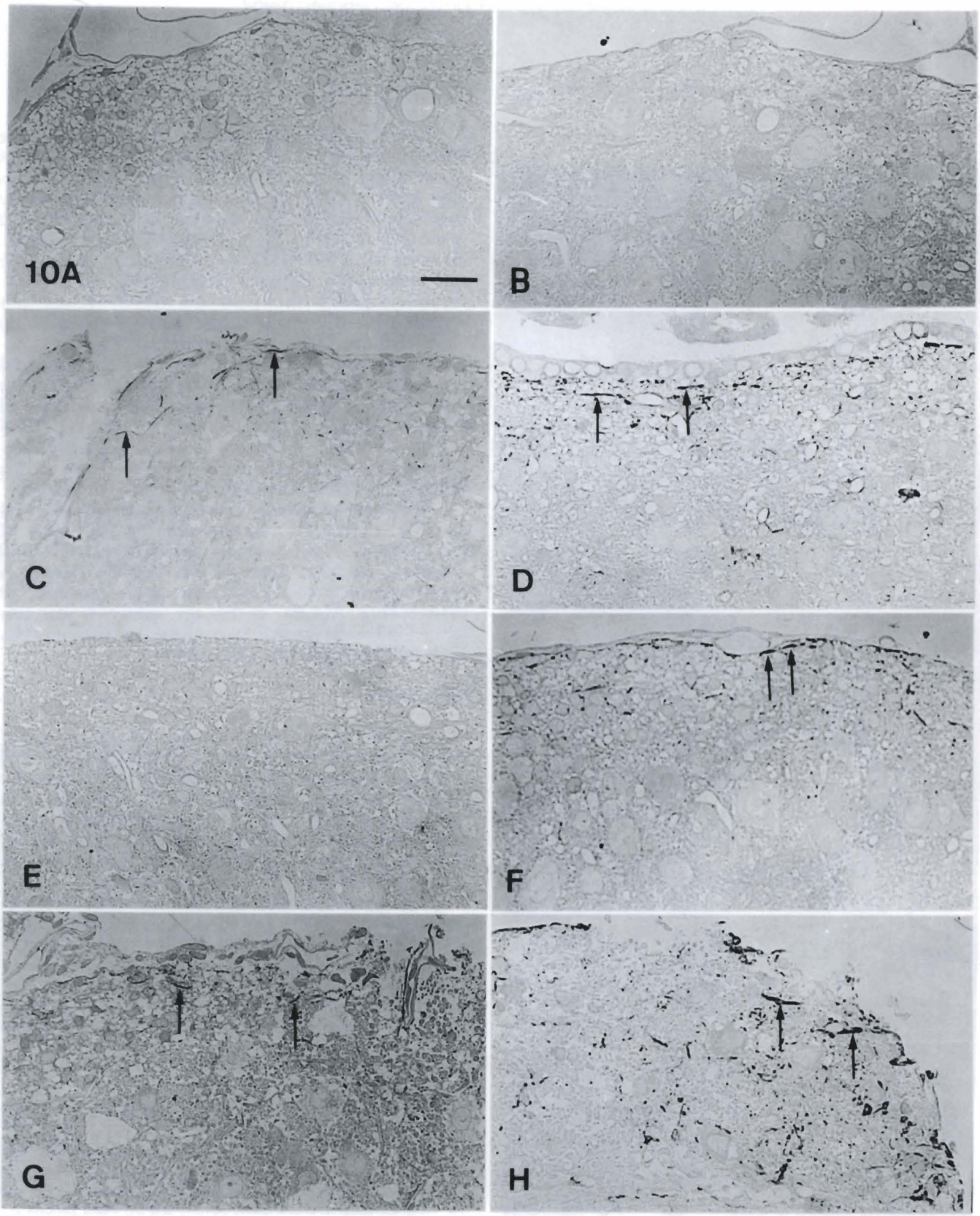

Fig. 10. Light micrographs of GFAP-IR in the superficial layer of the left **(A, C, E, G)** and right **(B, D, F, H)** AVCN. GFAP-IR is not immunolabeled in the left **(A)** and right **(B)** AVCN at one month after right ligation. GFAP-IR is immunolabeled in the left **(C)** and right **(D)** AVCN. GFAP-IR is immunolabeled more intensely in the right AVCN **(D)** than in the left **(C)**. At six months after right ligation, GFAP-IR is not immunolabeled in the left AVCN **(E)** but is slightly reduced in the right **(F)**. At nine months after right ligation, GFAP-IR is immunolabeled in the left AVCN **(G)** and in the right **(H)**. GFAP-IR is immunolabeled more intensely in the right AVCN **(H)** than in the left **(G)**. Scale bar: 25 μm.

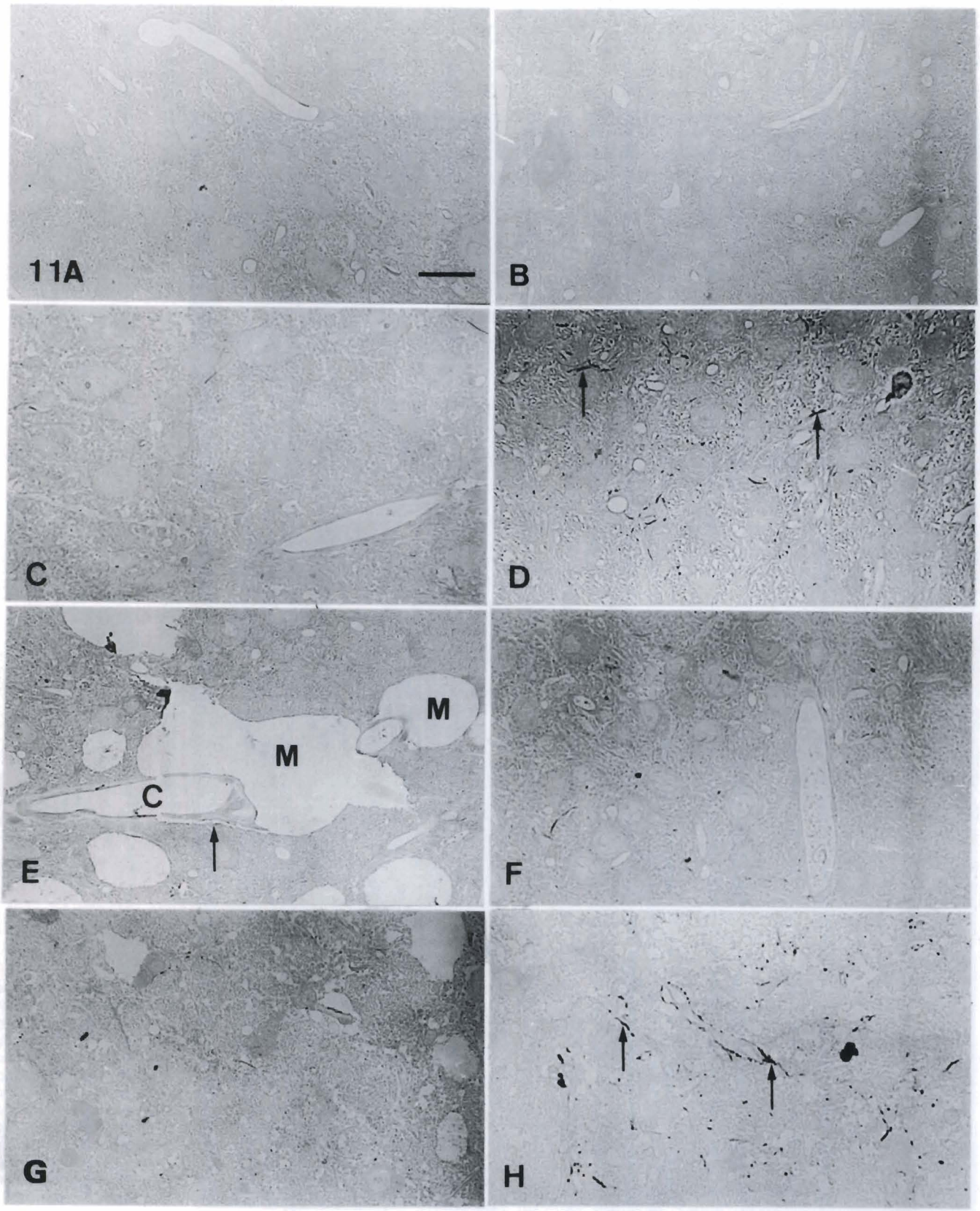

Fig. 11. Light micrographs of GFAP-IR in the deep layer of the left **(A, C, E, G)** and right **(B ,D, F, H)** AVCN. No discernible GFAP-IR is immunolabeled in the left **(A)** or right **(B)** AVCN at one month after right ligation. At three months after right ligation, GFAP-IR is not immunolabeled in the left AVCN **(C)** but is immunolabeled in the right **(D)**. At six months after right ligation, no discernible GFAP-IR is immunolabeled in the left **(E)** or right **(F)** AVCN. At nine months after right ligation, GFAP-IR is not immunolabeled in the left AVCN **(G)** but is immunolabeled in the right **(H)**. Scale bar: 25 μm.

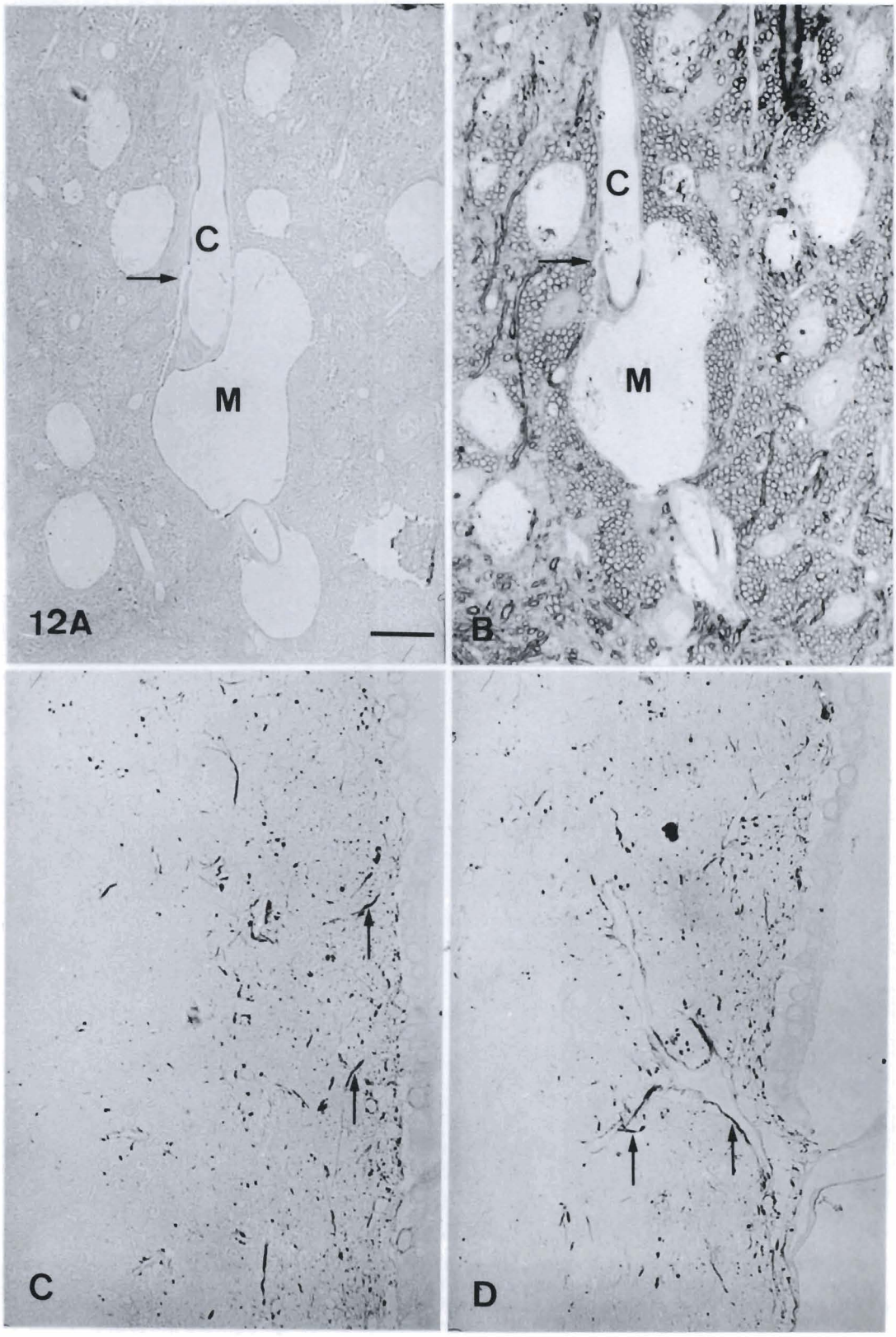

Fig. 12. Light micrographs at six months after right ligation. A microcyst (M) in the left AVCN is closely associated with blood vessels (C) in the deep layer of the AVCN. The microcyst connect with the blood vessel through a leakage route or channel (arrow) **(A)**. The adjacent semi-thin section is stained with toluidine blue **(B)**. GFAP-IR (arrows) is also located in the ependymal layer of the left **(C)** and right **(D)** AVCN. Scale bar: 25 μm.

between 5 weeks and 18 months of age. The location of microscysts are either within the neuronal cells or within the neuropil of the cochlear nuclei. One kind of microcyst is probably formed by the fusion of foamy regions or the distension (protrusion) of the myelinated nerve fiber. Another kind of microcyst contains membranous septa including many vesicles. It has been previously postulated that the membranous structures are presumably derived from retracted axons or the detachment of the myelin sheath. The vesicles are likely to be a transitory form of degenerating mito-chondria or a disruption of the myelin sheath. The present work has demonstrated that external auditary canal occlusion caused a severe change in the myelin sheath including detachment of the myelin sheath from the retracted axons, protrusion of the myelin sheath, and disruption in the myelin sheath. This finding suggests that the myelin sheath is probably the major source for the formation of microcysts, especially for large vesiculated microcysts.

Microcysts are not histologically stained either with basic or acidic dyes, or with the Sudan black B stain (Ostapoff and Morest, 1989), or with GFAP (Faddis and McGinn, 1993). There is also no apparent astroglial response (McGinn and Faddis, 1987; Ostapoff and Morest, 1989). By using immunocytochemical markers for astrocytes and oligodendrocytes, Czibulka and Schwartz (1993) have demonstrated a high correlation between astrocytic processes and microcysts. Their results indicate that up to 80% of microcysts are either contacted by astrocytic profiles over much of their perimeter or are labeled internally by astrocytic markers S-100 (the glial calcium-binding protein) or GFAP (the astroglia-specific cytoskeletal protein). Our findings further demonstrated that with increasing age GFAP-IR was intensely immunolabeled in the ipsilateral AVCN after surgical monaural ligation. Moreover, there was a consistent inverse relationship between an increase in GFAP-IR and a decrease in microcysts. One assumption we made for this fact was that astrocytes were likely to be involved in regulating the depletion of the microcysts after external auditory canal occlusion by surgical ligation.

Previous investigations have demonstrated that the appearance of microcysts in the gerbil PVCN cannot result from the selective loss of any single class of neurons (Czibulka and Schwartz, 1991). They indicate that microcysts are not neurons with cavities but are probably glial structures capable of rapid expansion or shrinkage as a result of some dynamic process related to controlling the extracellular environment around them. Changes in the extracellular environment triggering the formation or loss of fluid filled cavities are related to stimulation of the auditory pathway. Indeed, a significant age-related decrease in oligodendrocyte density is found in the PVCN but no difference is found in the AVCN (Faddis and McGinn, 1993). Other possible causes of microcysts are suggested from the axonal structure (Ostapoff and Morest, 1989). Unfortunately, nothing is known about the origin and regulatory mechanism of microcysts, but their locations along blood vessels, together with communication through a leakage route or channel, suggests that microcysts may be associated with functional changes in the blood vessel. A surprising finding was that the multivesicular bodies in the pericyte were associated with the presence of a membranous structure in the lumen of the blood vessel. A likely explanation for our results is that the clearance and depletion of the microcysts around the blood vessel may be transported by vacuoles through the cytoplasm of the endothelial cell. The pericyte surrounding the blood vessel may induce damage in the blood brain barrier. A membranous structure, contents of the microcysts, partially enters the lumen of the blood vessel through a leakage route or channel. Therefore, this progressive movement results in the retention of a membranous structure in the lumen of the blood vessel and in the neuropil.

The appearance of a leakage route or channel between a blood vessel and a microcyst was a surprise. The change in the wall of the blood vessel may be explained by a similar mechanism of the disruption of the blood brain barrier. Previous studies have demonstrated that blood vessel wall damage causes the breakdown of the blood-brain barrier with consequent chronic vasogenic brain edema in cold injury (Tengvar and Olsson, 1982; Bothe et al., 1984; Tengvar, 1986), in polycystic lipomembranous osteodysplasia and sclerosing leukoencephalopathy (PLO-SL) (Kalimo et al., 1994), and in stroke-prone spontaneously hypertensive rats (Fredriksson et al., 1985). It has also been reported that macrophages and astrocytes may be involved in this damage. Macrophages induce the release of vasoactive amines which cause vasospasm leading to an increase in vascular permeability and destroying the blood brain barrier (Cammer et al., 1978). Astrocytes can be induced to generate and release lipoxygenase derivative leukotriene C_4 from arachidonate conversion (Hartung and Toyka, 1987). Previous investigations have demonstrated that leukotriene breaks down the blood-brain barrier and induces the formation of brain edema (Black and Hoff, 1985; Black et al., 1986). In this study, we have shown that the GFAP-IR is closely associated with the blood vessel. Astrocytes may play a regulatory role in the depletion of microcysts to maintaining the homeostasis of the microenvironment in the cochlear nuclei.

Acknowledgments. This work was supported by the National Science Council (Grants No. NSC82-0412-B-010-075, NSC83-0412-B-010-027 and NSC84-0412-B-010-021), Taipei, Taiwan, Republic of China.

References

Bignami A., Eng L.F., Dahl D. and Uyeda C.T. (1972). Localisation of the glial fibrillar acidic protein in astrocytes by immunofluorescence. Brain Res. 43, 429-435.

Black K.L. and Hoff J.T. (1985). Leukotrienes increase blood-brain

barrier permeability following intraparenchymal injections in rats. Ann. Neurol. 18, 349-351.

Black K.L., Hoff J.T., McGillicuddy J.E. and Gebarski S.S. (1986). Increased leukotriene C_4 and vasogenic edema surrounding brain tumors in humans. Ann. Neurol. 19, 592-595.

Bothe H.W., Bodsch W. and Hossmann K.-A. (1984). Relationship between specific gravity, water content and serum protein extravasation in various types of vasogenic brain edema. Acta Neuropathol. (Berl) 64, 37-42.

Butt A.M. and Kirvell S. (1996). Glial cells in transected optic nerves of immature rats. II. An immunohistochemical study. J. Neurocytol. 25, 381-392.

Cammer W., Bloom B.R., Norton W.T. and Gordon S. (1978). Degradation of basic protein in myelin by neutral proteases secreted by stimulated macrophages: A possible mechanism of inflammatory demyelination. Proc. Natl. Acad. Sci. USA 75, 1554-1558.

Czibulka A. and Schwartz I.R. (1991). Neuronal populations in the gerbil PVCN: effects of age, hearing status and microcysts. Hearing Res. 52, 43-58.

Czibulka A. and Schwartz I.R. (1993). Glial or neuronal origin of microcysts in the gerbil PVCN? Hearing Res. 67, 1-12.

Du S.J., Chiu M.M., Ku Y.R. and Yu S.M. (1994). Microcysts in the anteroventral cochlear nucleus of acoustically deprived gerbils. Proceedings of the 15th ROC Symposium on Electron Microscopy. pp 3-4.

Eng L.F., Vanderhaeghen J.J., Bignami A. and Gerstl B. (1971). An acidic protein isolated from fibrous astrocytes. Brain Res. 28, 351-354.

Faddis B.T. and McGinn M.D. (1993). Glial populations in the juvenile and adult Mongolian gerbil: relationship to spongioform degeneration of the ventral cochlear nucleus. Exp. Neurol. 120, 160-169.

Fredriksson K., Auer R.N., Kalimo H., Nordborg C., Olsson Y. and Johansson B.B. (1985). Cerebrovascular lesion in stroke-prone spontaneously hypertensive rats. Acta Neuropathol. (Berl) 68, 284-294.

Hartung H.-P. and Toyka K.V. (1987). Leukotriene production by cultured astroglial cells. Brain Res. 435, 367-370.

Kalimo H., Sourander P., Järvi O. and Hakola P. (1994). Vascular changes and blood-brain barrier damage in the pathogenesis of polycystic lipomembranous osteodysplasia with sclerosing leukoencephalopathy (membranous lipodystrophy). Acta Neurol. Scand. 89, 353-361.

Kitzes L.M. and Moore H.C. (1989). Cavitation in the adult gerbil ventral cochlear nucleus is reversed by cochlear ablation. Abstr. Assoc. Res. Otolaryngol. 15, 743.

McGinn M.D. and Faddis B.T. (1987). Auditory experience affects degeneration of the ventral cochlear nucleus in mongolian gerbils. Hearing Res. 31, 235-244.

McGinn M.D. and Faddis B.T. (1988). Acoustic isolation reduces spongioform degeneration of the cochlear nuclei in gerbils. Abstr. Assoc. Res. Otolaryngol. 10, 208-209.

McGinn M.D., Faddis B.T. and Moore H.C. (1990). Acoustic isolation reduces degeneration of the ventral cochlear nuclei in mongolian gerbils. Hearing Res. 48, 265-274.

McLean W. and Nakane P.F. (1974). Periodate-lysine-paraformaldehyde fixative. A new fixative for immunoelectron microscopy. J. Histochem. Cytochem. 22, 1077-1083.

Morest D.K., Ostapoff E.-M., Feng J. and Kuwada S. (1986). Intracellular recordings of acoustic responses of identified cell types in the cochlear nucleus of the Mongolian gerbil and signs of a naturally occurring disease of the auditory system. IUPS Satellite Symposium on Hearing. Univ. California. San Francisco. p 80.

Ostapoff E.-M. and Morest D.K. (1989). A degenerative disorder of the central auditory system of the gerbil. Hearing Res. 37, 141-162.

Ostapoff E.-M., Morest D.K., Feng J. and Kuwada S. (1987). A degenerative disease of the auditory system of the gerbil, *Meriones* sp. Abstr. Assoc. Res. Otolaryngol. 10, 209.

Riggs G.H., Cooper N.G.F. and Schweitzer L. (1995). Patterns of GFAP-immunoreactivity parallel the tonotopic axis in the developing dorsal cochlear nucleus. Hearing Res. 90, 89-96.

Schwartz I.R. and Karnofsky R. (1988). "Holes" in the gerbil auditory system do not cause major changes in neuronal populations in the PVCN. Abstr. Soc. Neurosci. 14,491.

Statler K.D., Chamberlain S.C., Slepecky N.B. and Smith R.L. (1990). Development of mature microcystic lesions in the cochlear nuclei of the Mongolian gerbil, *Meriones unguiculatus*. Hearing Res. 50, 275-288.

Tengvar C. (1986). Extensive intraneuronal spread of horseradish peroxidase from a focus of vasogenic edema into remote areas of central nervous system. Acta Neuropathol. (Berl) 71, 177-189.

Tengvar C. and Olsson Y. (1982). Uptake of macromolecules into neurons from a focal vasogenic cerebral edema and subsequent axonal spread to other brain regions. Acta Neuropathol. (Berl) 57, 233-235.

Woolf N., Ryan A.F., Silva E., Keithley E. and Schwartz I.R. (1987). Functional and anatomical correlates of aging in the Mongolian gerbil auditory system. Abstr. Soc. Neurosci. 13, 1260.

Yu S.M. (1992). Postnatal development of GABAergic neurons in the gerbil cochlear nucleus: pre-embedding and post-embedding immunocytochemical staining. J. Formosan Med. Assoc. 91, 359-365.

Yu S.M. (1993a). Paraformaldehyde-lysine-periodate (PLP) and osmium fixation for correlating light and electron immunolabeling of prolactin cells. J. Histotechnol. 16, 125-128.

Yu S.M. (1993b). Prolactin immunoreactivity in the rat pituitary glands: comparison of immunofluorescence, immunoperoxidase, and immunogold techniques. J. Histotechnol. 16,323-328.

Yu S.M. and Du S.J. (1995). Morphologic changes in the anteroventral cochlear nucleus of acoustically-deprived gerbil. Proceedings of the 53rd Annual Meeting for Microscopy Society of America. pp 960-961.

Yu S.M. and Ke T.L. (1992). Microcysts in the gerbil cochlear nucleus. Proceedings of the 13rd R.O.C. Symposium on Electron Microscopy. pp 27-28.

Yu S.M. and Schwartz I.R. (1989). An improved flat embedding technique for immunoelectron microscopy. Stain Technol. 64, 143-146.

Accepted January 13, 1997